Carbon 148 (2019) 134–140

Contents lists available at ScienceDirect

Carbon

journal homepage: www.elsevier.com/locate/carbon

Commercial expanded graphite as high-performance cathode for low-cost aluminum-ion battery

Xiaozhong Dong [a, 1], Hanyan Xu [a, 1], Hao Chen [a], Liyong Wang [b], Jiaqing Wang [a], Wenzhang Fang [a], Chen Chen [a], Muhammad Salman [a], Zhen Xu [a], Chao Gao [a, *]

[a] MOE Key Laboratory of Macromolecular Synthesis and Functionalization, Department of Polymer Science and Engineering, Key Laboratory of Adsorption and Separation Materials & Technologies of Zhejiang Province, Zhejiang University, Hangzhou, 310027, PR China
[b] Hebei Normal University for Nationalities, Chengde, 067000, PR China

ARTICLE INFO

Article history:
Received 19 February 2019
Received in revised form
14 March 2019
Accepted 24 March 2019
Available online 25 March 2019

ABSTRACT

Aluminum-ion battery (AIB) is a very promising rechargeable battery system for its safety and three-electron-redox aluminum anode. However, the low cost-effectiveness and performance limit its practical application, thus requiring low-cost cathode-electrolyte system with large-scale manufacturing potential. In this work, we successfully achieved a low-cost and high-performance AIB system consisting of commercial expanded graphite (EG) cathode and $AlCl_3$-triethylamine hydrochloride ($AlCl_3$-ET) electrolyte. The assembled AIB exhibited the cathode capacity of 78.3 ± 4.1 mAh g^{-1} (156.6 ± 8.2 mAh cm^{-3}) at 5 A g^{-1} with 77.5% retention after 30 000 cycles. Even at a high active material loading of 6.16 mg cm^{-2}, the EG cathode displayed 101 mAh g^{-1} (207 mAh cm^{-3}) at 1 A g^{-1} with 95.5% retention after 11 500 stable cycles. We confirmed the part of the cathode capacity was contributed by $AlCl_4^-$ deposition, and the reaction mechanism of our new system resulted from the special structure of EG, which served as an important supplement of the classical mechanism of AIB. The high capacity of EG-AIB was contributed by $AlCl_4^-$ deposition and its stage 4 intercalation. This work provides a very promising and simple strategy for establishing the low-cost, high-performance and high-mass loading AIB system with great commercial value.

© 2019 Elsevier Ltd. All rights reserved.

1. Introduction

Aluminum-ion battery (AIB) has attracted much attention due to its nonflammability, low cost and high theory capacity of aluminum metal anode (2978 mAh g^{-1} and 8034 mAh cm^{-3}). Various types of AIB cathode materials have been extensively explored, such as carbon materials (CVD graphite foam [1,2], electrochemically-exfoliated graphite foam [2,3], pyrolytic graphite [4–6], natural graphite [7–13], exfoliated graphite [14,15] and graphene [16–22]), sulphur [23,24], chalcogenides [25–30] and MXene [31]. Among them, carbon materials are highly promising for fast charging and long cycling. Especially, graphene based cathode displayed an extremely high rate capability (111 mAh g^{-1} at 400 A g^{-1}), high cathode capacity (117 mAh g^{-1} at 5 A g^{-1}) and long cyclability (250 000 cycles) [18]. Whereas graphene is a relatively high-cost material due to the manufacturing complexity and energy consumption deriving from chemical reduction and high temperature annealing procedure. The graphitic carbon cathode material is deemed as an ideal choice in the purpose of large-scale application and industrialization of AIB. Within them, CVD and electrochemically-exfoliated graphite foams greatly suffer from milligram-scale productivity, which makes them difficult to satisfy the kilogram-scale and low-cost requirements from battery manufacture. By contrast, pyrolytic graphite and natural graphite cathodes do show good cost-effectiveness. But the cathode performance, especially rate capability and cycle life, are insufficient. Hence, seeking for a type of graphitic carbon material spontaneously satisfying high performance and low cost is of crucial importance. In addition, the commonly used ionic liquid electrolyte, which is a mixture of 1-ethyl-3-methylimidazolium chloride (EMI) with anhydrous aluminum chloride ($AlCl_3$), is fairly expensive as well. Despite previously proposed $AlCl_3$-urea [32,33], $AlCl_3$-NaCl [34,35], and $AlCl_3$-NaCl-KCl [36] electrolytes and $AlCl_3$ gel electrolyte [37] achieved higher cost-effectiveness, yet several

* Corresponding author.
E-mail address: chaogao@zju.edu.cn (C. Gao).
[1] Xiaozhong Dong and Hanyan Xu contributed equally to this work.

https://doi.org/10.1016/j.carbon.2019.03.080
0008-6223/© 2019 Elsevier Ltd. All rights reserved.

disadvantages such as high-temperature operation and insufficient performance limited their application. Therefore, finding out a low-cost and high-performance battery system, consisting of cheap cathode and electrolyte, is a key issue for the real achievement of commercialized AIB.

In this work, we established a totally low-cost AIB system, comprising of commercial expanded graphite (EG) cathode with low-cost $AlCl_3$-triethylamine hydrochloride ($AlCl_3$-ET) electrolyte. The assembled AIB exhibited the cathode capacity of 78.3 ± 4.1 mAh g^{-1} (156.6 ± 8.2 mAh cm^{-3}) at 5 A g^{-1} with 77.5% retention after 30 000 cycles. Significantly, the EG cathode, with a high loading of 6.16 mg cm^{-2}, displayed the specific capacity of 101 mAh g^{-1} (207 mAh cm^{-3}) at 1 A g^{-1} with 95.5% retention after 11 500 stable cycles. Besides, we offered a clear understanding of its battery mechanism, involved by not only $AlCl_4^-$ intercalation, but also $AlCl_4^-$ deposition. In a word, this work provided a perfect strategy for building the low-cost and high-performance AIB system, which would pave the way for the mass production of AIB.

2. Experimental

2.1. Preparation of the EG cathode film

We selected commercial EG (expanding rate of 500 by 1237 K treating, no sulphur involved, Hangzhou Gaoxi Technology Co. Ltd., China) as AIB cathode. The as-received wormlike EG was directly compressed into the free-standing electrode film with area loading about 2 mg cm^{-2} and the thickness about 10 μm, by virtue of its good self-adhesive property. Also, the EG powder/PVDF (mass ratio of 9/1) composite electrode film was prepared by coating method [38]. Its mass loading reached 6.16 mg cm^{-2} with the coating thickness about 30 μm.

2.2. Material characterization

EG was characterized by scanning electron microscope (SEM, Hitachi S4800), transmission electron microscope (TEM, JEM-2100), X-ray diffractormeter (XRD, BRUKER D8), Raman spectrometer (RENISHAW inVia-Reflex) and surface area & porosity analyzer (ASAP 2020 HD88). The EG cathode film at fully charged state was also characterized by the above instruments. The transparent cell for *in situ* Raman spectra was assembled by a glass slide with a cover glass.

2.3. Battery assembly

The EG cathode film was punched into circular plates with the diameter of 1 cm. In the argon-filled glovebox, the CR2025 coin cell was assembled with the above plate as the working electrode, aluminum foil (thickness/20 μm, Taiyuan Lizhiyuan Battery Sales Department) as the counter and reference electrode, $AlCl_3$-EMI (mole ratio of 1.3/1) and $AlCl_3$-ET (mole ratio of 1.5/1) mixtures as electrolytes, and glass fibre membrane (Whatman 934-AH) as the separator. The two electrolytes were prepared according to the method [16,19]. The only pouch cell for battery demonstration was assembled with a 4 cm × 6 cm EG cathode film.

2.4. Electrochemical measurement

The cyclic voltammetry (CV) test was scanned at 1 mV s^{-1} on a CHI660E workstation. The electrochemical impedance spectroscopy (EIS) was recorded from 10^5 to 0.01 Hz on the same CHI660E workstation. The cycling performance and rate capability of coin cells and the pouch cell were conducted on a LAND battery test system. The cutoff voltage ranges were 0.70–2.51 V for $AlCl_3$-EMI electrolyte and 0.70–2.54 V for $AlCl_3$-ET electrolyte.

3. Results and discussion

3.1. Characterization of the EG material

The appearance of the used EG is loose, porous and wormlike, as shown in Fig. 1a, which makes it self-adhesive and easy to process. Its elemental composition includes about 83% C content and 17% O content shown in Fig. S1. The line resistance of the directly-compressed EG film is about 2.99 Ω cm^{-1} presented in Fig. S2. EG curved surfaces (Fig. 1b) are composed of graphite sheets with dozens of layers (Fig. 1c). The XRD pattern (Fig. 1d) shows a sharp C (002) peak at $2\theta = 26.56°$ (the interlayer space, d = 0.3353 nm) yet no amorphous peak, indicating the graphite lattices are perfect with few defects. Besides, the Raman result (Fig. 1e) presents a high graphitization degree with the I_D/I_G ratio of 0.2878. Such perfect graphite lattices can benefit the intercalation of active species [16,18]. It is also demonstrated, by nitrogen adsorption method, that EG has a large BET special surface area of 54.16 m^2 g^{-1}, and pores with 3 nm and 40 nm diameter contribute the major special surface area and pore volume (Fig. 1f). The large special surface area and hierarchical pore structure are conducive to the infiltration of the electrolyte and the fast diffusion of intercalated ions [5,6].

3.2. Electrochemical performance of the EG cathode

Then, we employed the directly-compressed EG film as the cathode, aluminum foil as the anode, and the classical $AlCl_3$-EMI electrolyte, to assemble coin cells for testing the AIB electrochemical performance. As shown in Fig. 2a, at the current density of 1 A g^{-1}, the EG-EMI cell exhibited an initial stable capacity of 85.3 ± 0.7 mAh g^{-1}, yet decayed to 60 mAh g^{-1} after 3000 cycles. When the current density was increased to 5 A g^{-1}, the initial stable capacity of the EG-EMI cell dropped to 58.2 ± 4.1 mAh g^{-1}, but still comparable to other graphite cathodes [1,3,4,7,9,10], and the cell afforded 10 000 cycles. It can be clearly seen that the battery capacity underwent three stages: an initial increase, a stable cycling and a late decay [38]. At the initial stage, with the successive intercalation and deintercalation of $AlCl_4^-$, the EG sheets were exfoliated gradually [3,39,40] and thereby interlayers accommodated more $AlCl_4^-$, resulting in an increase of capacity. Whereas such electrochemical exfoliated behaviour inevitably caused the damage to the integrity of electrode structure, finally leading to the capacity fade [41]. From the rate capability (Fig. 2b), the EG-EMI cell hardly withstood a large current density, resulting from the relatively lower exfoliation degree of EG than that of graphene [1,7,10,16,20,22]. Compared with other graphite cathodes of AIB (Table S1), consequently, the EG cathode achieved a fairly good electrochemical performance.

In our purpose of establishing a cost-effective AIB system, employing cheap cathode material is far from enough, since the mostly used $AlCl_3$-EMI electrolyte is expensive. According to our previous study [19], the proposed novel $AlCl_3$-ET electrolyte, not only cost far less than $AlCl_3$-EMI electrolyte, but also could achieve the comparable performance with $AlCl_3$-EMI electrolyte. However, this newly-proposed electrolyte only combinated with the expensive graphene cathode. Therefore, we established the low-cost (double-cheap) system comprised of the EG cathode and $AlCl_3$-ET electrolyte. As shown in Fig. 2c, the capacity of the EG-ET cell increased by 15.6% and achieved 98.6 ± 0.7 mAh g^{-1} at 1 A g^{-1} with 5000 cycles. At 5 A g^{-1}, the capacity of the EG-ET cell improved by 34.5% and delivered 78.3 ± 4.1 mAh g^{-1} (156.6 ± 8.2 mAh cm^{-3},

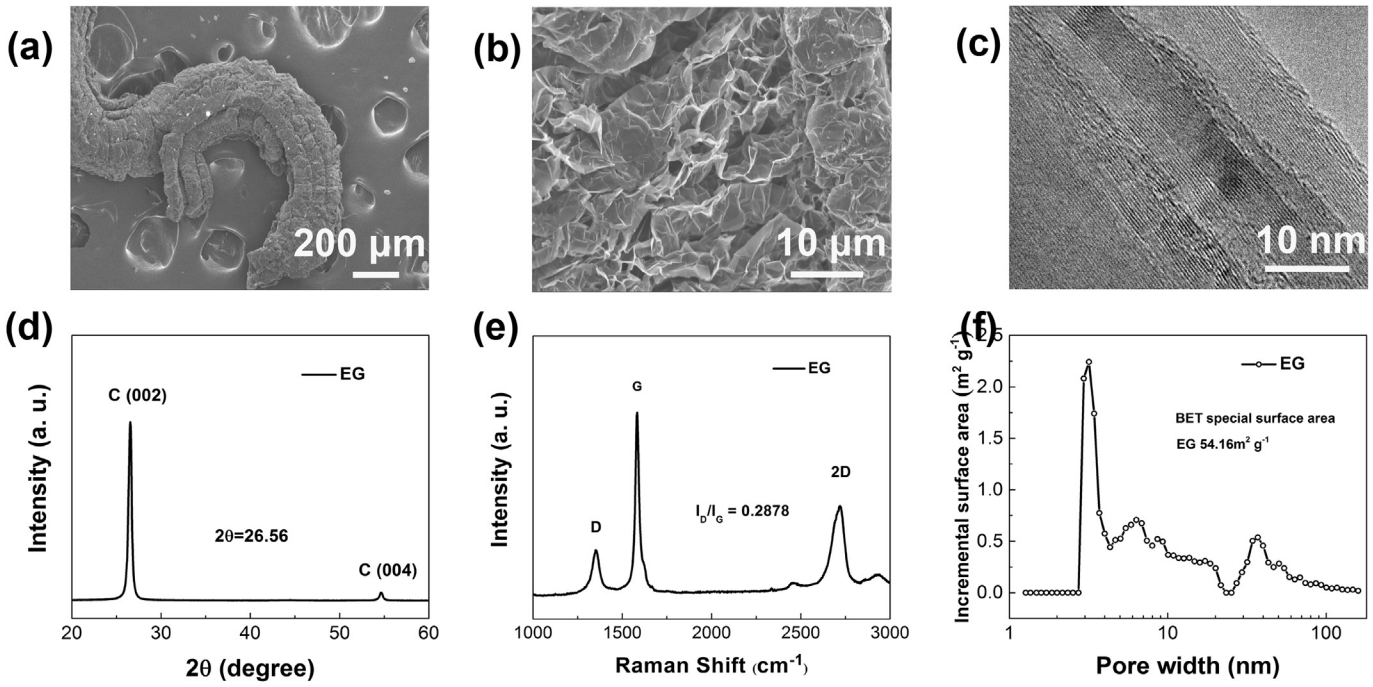

Fig. 1. Material characterization of the as-received EG. (a) the wormlike EG, (b) SEM image, (c) TEM image, (d) XRD pattern, (e) Raman spectra, (f) pore diameter distribution curve measured by nitrogen adsorption method. The commercial EG available in large quantities can be referred to Fig. S3. Pore diameter distribution in (f) can be further referred to Fig. S4.

based on the compressed film with the density of ~2 g cm^{-3}) with 77.5% retention after 30 000 cycles. In addition, the EG-ET cell also hardly tolerated a high current density of 8 A g^{-1} (Fig. 2d). Apparently, the EG-ET battery system displayed a higher capacity and more cycles than the EG-EMI case, which should be attributed to its higher electrolyte mole ratio (1.5/1), and its high coulombic efficiency within the broader cut-off voltage window of 0.70–2.54 V. Another important factor is that, the EG-EMI system had a higher potential compared to the EG-ET system, will be further discussed in CV results. It can be seen that the totally low-cost AIB system has been successfully built.

To verify the effectiveness of the above low-cost EG-ET AIB system, we assembled the pouch cell with EG cathode film which has a 30-times larger area than that of the working electrode in coin cell. The pouch cell also outputted the capacity of 80 mAh g^{-1} at 1 A g^{-1}, and lighted up a group of 31 LED lamps (Fig. 2e). However, it is still insufficient, since the above performance were obtained on the basis of the low area loading of 2 mg cm^{-2}. This will have none practicability unless the mass loading can be promoted more. Accordingly, by appropriate coating method, we prepared the EG powder/PVDF (mass ratio of 9/1) composite cathode film and improved the area loading to 6.16 mg cm^{-2}. The assembled coin cell exhibited the capacity of 101 mAh g^{-1} (207 mAh cm^{-3}, based on the coating film with the density of 2.05 g cm^{-3}) at 1 A g^{-1} with 95.5% retention after 11 500 stable cycles, as shown in Fig. 2f. As a result, such high area loading, low-cost cathode & electrolyte and excellent electrochemical performance fully indicate that the proposed EG-ET AIB system is very promising for commercialization.

3.3. Operating mechanism of the EG-ET AIB system

Except successfully building the low-cost and high-performance AIB system, the battery operating mechanism was also illustrated through the structure change of EG cathode during charge and discharge. The classic AIB operating mechanism [1] proposed by Dai's group was that $AlCl_4^-$ intercalated into cathode material and $Al_2Cl_7^-$ deposited on aluminum anode in the charging process; the quantity of $AlCl_4^-$ and $Al_2Cl_7^-$ existed a balance in the electrolyte (Fig. S7). In fact, this type of AIB is not a rocking-chair battery. $AlCl_4^-$ intercalation into graphite cathode in the stage 4 afforded the capacity of 60 mAh g^{-1} for AIB [1,7]. However, the EG-ET AIB showed a higher capacity than 60 mAh g^{-1}. We observed the phenomenon of $AlCl_4^-$ deposition on the surface of EG cathode in fully charged state, and confirmed that $AlCl_4^-$ deposition contributed the rest capacity. Thus, the existing battery mechanism for AIB was extended.

3.3.1. Intercalation behaviour of $AlCl_4^-$

Ex situ XRD patterns of the EG cathode film were studied at the fully charged state. All tests were conducted after the EG cathode reached a stable capacity. As shown in Fig. 3a, for the EG cathode of EG-ET system, the C (002) peak at $2\theta = 26.56°$ (d = 0.3353 nm) split into two peaks at $2\theta = 22.74°$ ($d_1 = 0.3907$ nm) and 27.64° ($d_2 = 0.3224$ nm), and the ratio of the corresponding interlayer space (d_1/d_2) is 1.21, consistent with the stage 4 intercalation of $AlCl_4^-$ [1,7,42]. However, the C (002) peak of EG-EMI system only shifts a little. Thus, the intercalation behaviour in EG-EMI system is relatively incomplete compared with that happened in EG-ET system, which also indicated the reason resulting in the gap of their capacities. Additionally, the d values of two new peaks emerged in fully charged state reflected the formation of highly strained graphite sheets due to $AlCl_4^-$ intercalation [1,7]. At the same time, it indicated that $AlCl_4^-$ (original size about 0.528 nm) intercalated into the EG interlayer in a distorted state.

Further, *in situ* Raman spectra of the EG cathode film were obtained by encapsulating cells in transparent glass. It should be noted that, during the formation of the graphite intercalation compound (GIC), the graphite G band will split into a lower-frequency component (E_{2g2}(i) mode) for vibrations of carbon atoms in un-intercalated graphite layer, and a higher-frequency

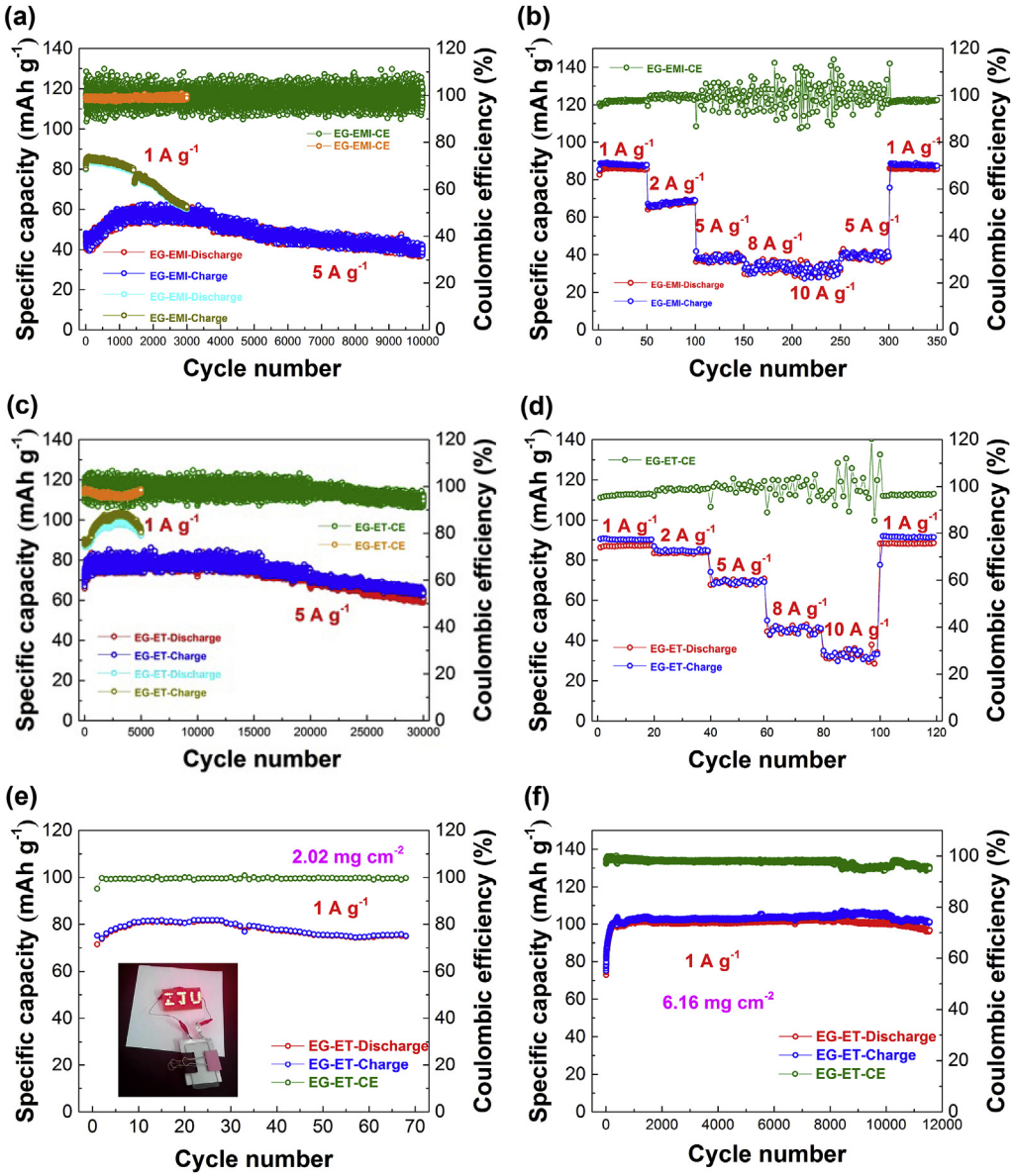

Fig. 2. EG-AIB electrochemical performance with EMI and ET electrolytes. (a) and (b) cycling performance and rate capability of EG-EMI system, (c) and (d) cycling performance and rate capability of EG-ET system, (e) cycling performance of the pouch cell (EG-ET system), (f) cycling performance of EG-ET system with a high mass loading of 6.16 mg cm^{-2}. The cutoff voltage ranges are 0.70–2.51 V for EMI electrolyte and 0.70–2.54 V for ET electrolyte. CE means coulombic efficiency. Voltage-capacity curves of two systems can be further referred to Figs. S5 and S6. (A colour version of this figure can be viewed online.)

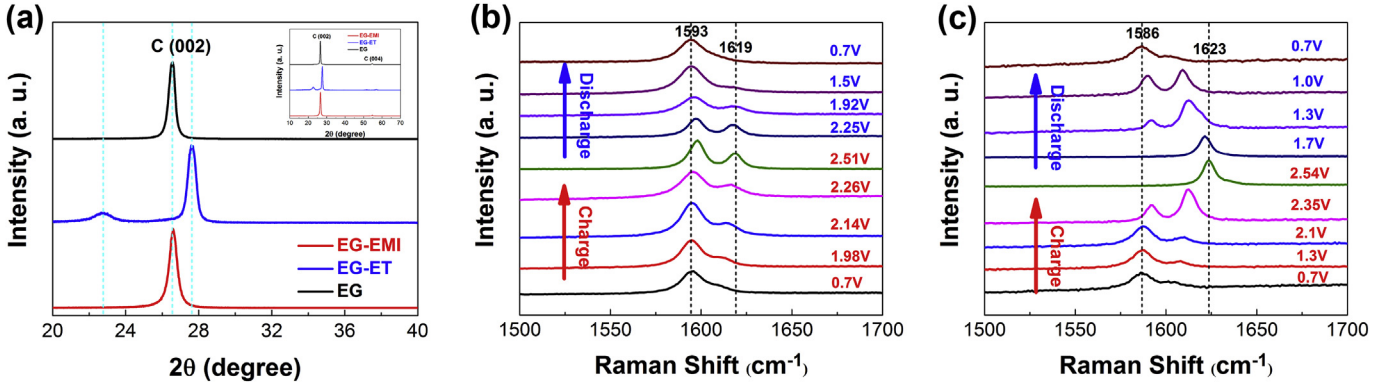

Fig. 3. (a) *ex situ* XRD patterns of EG cathode film at the fully charged state, (b) and (c) *in situ* Raman spectra of EG cathode film in EG-EMI and EG-ET system during charge and discharge. (A colour version of this figure can be viewed online.)

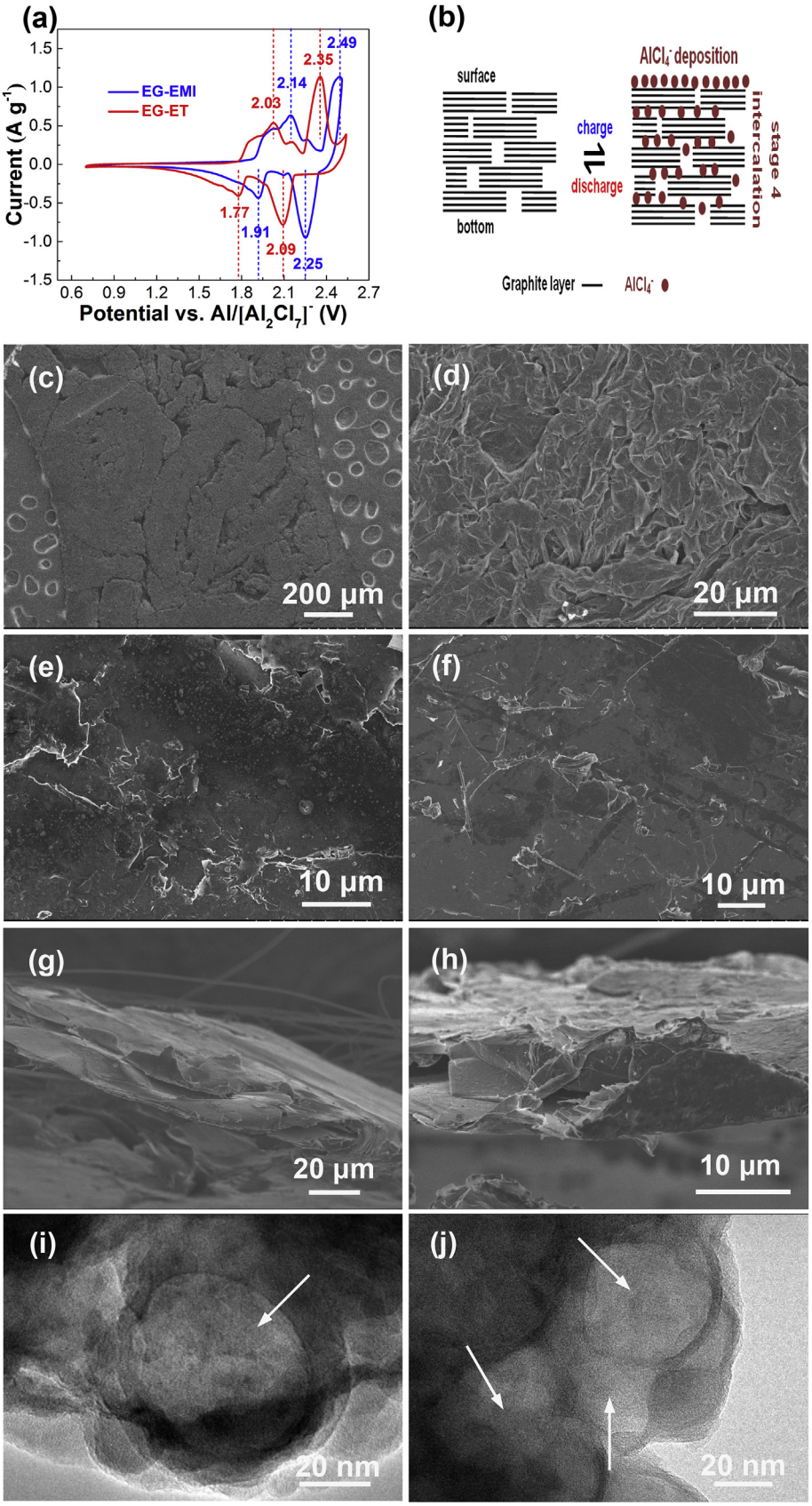

Fig. 4. (a) CV curves scanned at 1 mV s^{-1}, (b) schematic of $AlCl_4^-$ deposition and intercalation during charging process, (c) and (d) SEM images of the original EG cathode film with different scales, (e) and (f) SEM images of the cathode surface in EG-EMI and EG-ET system, (g) and (h) SEM images of the cathode cross-section in EG-EMI and EG-ET system, (i) and (j) TEM images of the cathode material in EG-EMI and EG-ET system. Samples of (e)~(j) were characterized at the fully charged state. (A colour version of this figure can be viewed online.)

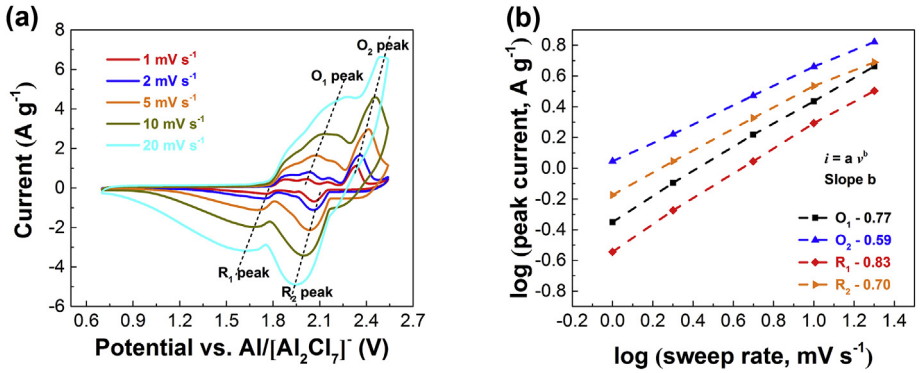

Fig. 5. (a) CV curves of EG-ET system with deferent sweep rates, (b) Logarithmic curve of peak current versus sweep rate from (a). (A colour version of this figure can be viewed online.)

component (E_{2g2}(b) mode) for vibrations of carbon atoms in intercalated graphite layer [1,7]. As shown in Fig. 3c, the Raman peak of EG-ET system changed from 1586 cm^{-1} (E_{2g2}(i) mode) to 1623 cm^{-1} (E_{2g2}(b) mode), and then returned back to 1586 cm^{-1} during charge and discharge, corresponding to $AlCl_4^-$ intercalation into and deintercalation from graphite sheets [7]. Whereas, as for EG-EMI system (Fig. 3b), the peak position at 1593 cm^{-1} (E_{2g2}(b) mode, maybe induced by the irreversible intercalation of $AlCl_4^-$) almost unchanged, yet the peak at 1619 cm^{-1} (E_{2g2}(b) mode) gradually strengthened and then disappeared during charge and discharge. This also confirmed that the extent of intercalation behaviour in EG-EMI system differed from the case in EG-ET system. Clearly, by Raman and XRD results, it is reasonable assumed that the ability of $AlCl_4^-$ intercalation into graphite interlayer in EG-ET system is stronger than in EG-EMI system. These newly observed phenomena would help us to deepen the understanding of the intercalation process.

3.3.2. Deposition behaviour of $AlCl_4^-$

In addition, it is noteworthy that, according to previous reports [1,3,7,42], the stage 4 intercalation of $AlCl_4^-$ offered the capacity of 60 mAh g^{-1} for AIB. Nevertheless, AIB capacities here are much higher than 60 mAh g^{-1}. We use CV curves and morphology change of the EG cathode film to illustrate the reason.

From CV curves (Fig. 4a), it can be seen that, the sharp oxidation peaks appeared at 2.49 V for EG-EMI system and at 2.35 V for EG-ET system, corresponding to the stage 4 $AlCl_4^-$ intercalation into graphite interlayer. While there existed hump oxidation peaks at 2.14 V for EG-EMI system and at 2.03 V for EG-ET system, which are assumed to partly correspond to $AlCl_4^-$ deposition on the surface of EG during charging process (Fig. 4b).

In order to verify this assumption, we studied cathode microstructures at the original and fully charged state. From the morphology of the original EG film, it can be observed that the obvious self-adhesive traces (Fig. 4c) and many wrinkles stacked by graphite sheets on the surface (Fig. 4d). At the fully charged state, all wrinkles on EG electrode surfaces disappeared, emerging a flat surface, which is actually caused by $AlCl_4^-$ deposition (Fig. 4e and f). And cross-section images (Fig. 4g and h) reflect that the interior of the electrode is tightly stacked by graphite planes (compressed from EG curved surfaces). Besides, Fig. 4i and j show TEM images at the fully charged state. Although no clear lattice fringe was observed due to the shielding from $AlCl_4^-$, interestingly, a special structure of hollow cavity (indicated by arrows) is ubiquitously existed. On one hand, the hollow cavity provided the location of $AlCl_4^-$ deposition; on the other hand, the cavity wall, composed of graphite sheets, could be intercalated [43]. Thus, due to the high special surface area of EG ($AlCl_4^-$ deposition on electrode surfaces) and the special cavity structure forming during cycling ($AlCl_4^-$ deposition in hollow cavities), $AlCl_4^-$ deposition was confirmed to contribute the rest AIB capacity (Fig. 4b).

For further discussing the capacity contribution of $AlCl_4^-$ deposition, we presented CV curves of the EG-ET system with deferent sweep rates. In Fig. 5a, compared with O_2 peaks ($AlCl_4^-$ intercalation), the relative intensity of O_1 peaks ($AlCl_4^-$ deposition) enlarged as the increase of the sweep rate. It indicated that the increase of the sweep rate promoted the reaction kinetics of depositing $AlCl_4^-$ more than that of intercalating $AlCl_4^-$, consistent with the fast deposition of $AlCl_4^-$ on EG surfaces with a large BET special surface area. By virtue of the formula ($i = av^b$) for distinguishing the charge storage mechanism proposed by Simon. *et al.* [44], b = 0.5 reflected the battery behaviour of 100% and b = 1 reflected the supercapacitor behaviour of 100%. From Fig. 5b, b = 0.59 for O_2 peak, indicated that the reaction of the O_2 peak belonged to the battery mechanism. Combined with *ex situ* XRD results (Fig. 3a), it can be confirmed that the sharp oxidation peak (O_2 peak) corresponded to the stage 4 $AlCl_4^-$ intercalation. While b = 0.77 for O_1 peak, it proved that the reaction of the hump oxidation peak (O_1 peak) was close to, but different with the supercapacitor mechanism. That is, [$AlCl_4$] existed on EG electrode surfaces at the fully charged state, rather than $AlCl_4^-$ adsorbed on EG electrode surfaces. The detailed AIB mechanism still needs to be further studied in experimental and theoretical aspects.

In addition, one important factor mentioned above (Section 3.2) is that the potential difference of the EG-EMI system relative to the EG-ET system. From Fig. 4a, no matter the sharp oxidation peak ($AlCl_4^-$ intercalation) or the hump oxidation peak ($AlCl_4^-$ deposition), the potential decrease of 0.11–0.14 V made it easier to conduct $AlCl_4^-$ intercalation and deposition in the EG-ET system, and thus enhanced the charge storage ability. Whereas the higher potential for $AlCl_4^-$ intercalation and deposition accelerated the destruction of cathode material structure in the EG-EMI system, resulting in the fast fading of the capacity. The potential difference was caused by properties of cations (EMI^+ and ET^+). This also indicated that the compatibility of cathode & electrolyte was crucial in AIB systems.

4. Conclusions

In summary, we used commercial EG cathode and $AlCl_3$-ET electrolyte to successfully fabricate a cost-effective, practical and high-performance AIB system. The battery exhibited the cathode capacity of 78.3 ± 4.1 mAh g^{-1} (156.6 ± 8.2 mAh cm^{-3}) and 30 000 times cycle life at 5 A g^{-1}. Even with a high loading of 6.16 mg cm^{-2},

it achieved 101 mAh g^{-1} (207 mAh cm^{-3}) at 1 A g^{-1} with 11 500 stable cycles. We extended the existing reaction mechanism of AIB. The total capacity of EG-AIB was contributed by $AlCl_4^-$ deposition and its stage 4 intercalation. This work provides a very promising strategy for preparing low-cost and high-performance AIB, which would pave the way for the commercialization of AIB.

Acknowledgements

The authors would like to acknowledge the support of the Key Research and Development Plan of Zhejiang Province (2018C01049), the National Natural Science Foundation of China (no. 51533008, no. 51703194 and no. 21805242), the National Key R&D Program of China (2016YFA0200200), the Hundred Talents Program of Zhejiang University (188020*194231701/113) and the Excellent Postdoctoral Special Fund of Zhejiang University for funding this research work.

Appendix A. Supplementary data

Supplementary data to this article can be found online at https://doi.org/10.1016/j.carbon.2019.03.080.

References

[1] M.C. Lin, M. Gong, B. Lu, Y. Wu, D.Y. Wang, M. Guan, et al., An ultrafast rechargeable aluminium-ion battery, Nature 520 (7547) (2015) 325–328.
[2] H. Dai, M.C. Lin, M. Gong, B. Lu, Y. Wu, Ultra-fast rechargeable metal-ion battery, U. S. patent 14/622 (2015) 692.
[3] Y. Wu, M. Gong, M.C. Lin, C. Yuan, M. Angell, L. Huang, et al., 3D graphitic foams derived from chloroaluminate anion intercalation for ultrafast aluminum-ion battery, Adv. Mater. 28 (41) (2016) 9218–9222.
[4] G.A. Elia, I. Hasa, G. Greco, T. Diemant, K. Marquardt, K. Hoeppner, et al., Insights into the reversibility of aluminum graphite batteries, J. Mater. Chem. A 5 (20) (2017) 9682–9690.
[5] N.P. Stadie, S.T. Wang, K.V. Kraychyk, M.V. Kovalenko, Zeolite-templated carbon as an ordered microporous electrode for aluminum batteries, ACS Nano 11 (2) (2017) 1911–1919.
[6] Z.A. Zafar, S. Imtiaz, R. Li, J. Zhang, R. Razaq, Y. Xin, et al., A super-long life rechargeable aluminum battery, Solid State Ionics 320 (2018) 70–75.
[7] D.Y. Wang, C.Y. Wei, M.C. Lin, C.J. Pan, H.L. Chou, H.A. Chen, et al., Advanced rechargeable aluminium ion battery with a high-quality natural graphite cathode, Nat. Commun. 8 (2017) 14283.
[8] Y.R. Gao, C.Q. Zhu, Z.Z. Chen, G. Lu, Understanding ultrafast rechargeable aluminum-ion battery from first-principles, J. Phys. Chem. C 121 (13) (2017) 7131–7138.
[9] G. Wang, M. Yu, J. Wang, D. Li, D. Tan, M. Loeffler, et al., Self-activating, capacitive anion intercalation enables high-power graphite cathodes, Adv. Mater. 30 (20) (2018) 1800533.
[10] H. Sun, W. Wang, Z. Yu, Y. Yuan, S. Wang, S. Jiao, A new aluminium-ion battery with high voltage, high safety and low cost, Chem. Commun. 51 (59) (2015) 11892–11895.
[11] S.Q. Jiao, H.P. Lei, J.G. Tu, J. Zhu, J.X. Wang, X.H. Mao, An industrialized prototype of the rechargeable Al/AlCl3-[EMIm]Cl/graphite battery and recycling of the graphitic cathode into graphene, Carbon 109 (2016) 276–281.
[12] K.V. Kraychyk, S. Wang, L. Piveteau, M.V. Koyalenko, Efficient aluminum chloride natural graphite battery, Chem. Mater. 29 (10) (2017) 4484–4492.
[13] S.T. Wang, K.V. Kravchyk, F. Krumeich, M.V. Kovalenko, Kish graphite flakes as a cathode material for an aluminum chloride-graphite battery, ACS Appl. Mater. Interfaces 9 (34) (2017) 28478–28485.
[14] A. Zhamu, B.Z. Jang, Aluminum secondary battery having an exfoliated graphite-based high-capacity cathode and manufacturing method, U. S. patent 15/434 (2017) 913.
[15] A. Zhamu, B.Z. Jang, Aluminum Secondary Battery Having an Exfoliated Graphite-Based High-Capacity Cathode and Manufacturing Method, PCT/US2018/016400, 2018.
[16] H. Chen, F. Guo, Y. Liu, T. Huang, B. Zheng, N. Ananth, et al., A defect-free principle for advanced graphene cathode of aluminum-ion battery, Adv. Mater. 29 (12) (2017) 1605958.
[17] H. Chen, C. Chen, Y.J. Liu, X.L. Zhao, N. Ananth, B.N. Zheng, et al., High-Quality graphene microflower design for high-performance Li-S and Al-ion batteries, Adv. Energy Mater. 7 (17) (2017) 1700051.
[18] H. Chen, H. Xu, S. Wang, T. Huang, J. Xi, S. Cai, et al., Ultrafast all-climate aluminum-graphene battery with quarter-million cycle life, Sci. Adv. 3 (12) (2017) eaao7233.
[19] H. Xu, T. Bai, H. Chen, F. Guo, J. Xi, T. Huang, et al., Low-cost AlCl3/Et3NHCl electrolyte for high-performance aluminum-ion battery, Energy Storage Mater. (2018), https://doi.org/10.1016/j.ensm.2018.08.003.
[20] L.Y. Zhang, L. Chen, H. Luo, X.F. Zhou, Z.P. Liu, Large-sized few-layer graphene enables an ultrafast and long-life aluminum-ion battery, Adv. Energy Mater. 7 (15) (2017) 1700034.
[21] S.C. Jung, Y.J. Kang, D.J. Yoo, J.W. Choi, Y.K. Han, Flexible few-layered graphene for the ultrafast rechargeable aluminum-ion battery, J. Phys. Chem. C 120 (25) (2016) 13384–13389.
[22] Q. Zhang, L. Wang, J. Wang, C. Xing, J. Ge, L. Fan, et al., Low-temperature synthesis of edge-rich graphene paper for high-performance aluminum batteries, Energy Storage Mater. 15 (2018) 361–367.
[23] G. Cohn, L. Ma, L.A. Archer, A novel non-aqueous aluminum sulfur battery, J. Power Sources 283 (2015) 416–422.
[24] H.C. Yang, L.C. Yin, J. Liang, Z.H. Sun, Y.Z. Wang, H.C. Li, et al., An aluminum-sulfur battery with a fast kinetic response, Angew. Chem. Int. Ed. 57 (7) (2018) 1898–1902.
[25] Y.X. Hu, B. Luo, D.L. Ye, X.B. Zhu, M.Q. Lyu, L.Z. Wang, An innovative freeze-dried reduced graphene oxide supported SnS2 cathode active material for aluminum-ion batteries, Adv. Mater. 29 (48) (2017) 1606132.
[26] Y.X. Hu, D.L. Ye, B. Luo, H. Hu, X.B. Zhu, S.C. Wang, et al., A binder-free and free-standing cobalt Sulfide@Carbon nanotube cathode material for aluminum-ion batteries, Adv. Mater. 30 (2) (2018) 1703824.
[27] T.H. Cai, L.M. Zhao, H.Y. Hu, T.G. Li, X.C. Li, S. Guo, et al., Stable CoSe2/carbon nanodice@reduced graphene oxide composites for high-performance rechargeable aluminum-ion batteries, Energy Environ. Sci. 11 (9) (2018) 2341–2347.
[28] S. Wang, S.Q. Jiao, J.X. Wang, H.S. Chen, D.H. Tian, H.P. Lei, et al., High-performance aluminum-ion battery with CuS@C microsphere composite cathode, ACS Nano 11 (1) (2017) 469–477.
[29] J.L. Jiang, H. Li, T. Fu, B.J. Hwang, X. Li, J.B. Zhao, One-dimensional Cu2-xSe nanorods as the cathode material for high-performance aluminum-ion battery, ACS Appl. Mater. Interfaces 10 (21) (2018) 17942–17949.
[30] L.X. Geng, G.C. Lv, X.B. Xing, J.C. Guo, Reversible electrochemical intercalation of aluminum in Mo6S8, Chem. Mater. 27 (14) (2015) 4926–4929.
[31] A. VahidMohammadi, A. Hadjikhani, S. Shahbazmohamadi, M. Beidaghi, Two-dimensional vanadium carbide (MXene) as a high-capacity cathode material for rechargeable aluminum batteries, ACS Nano 11 (11) (2017) 11135–11144.
[32] M. Angell, C.J. Pan, Y.M. Rong, C.Z. Yuan, M.C. Lin, B.J. Hwang, et al., High Coulombic efficiency aluminum-ion battery using an AlCl3-urea ionic liquid analog electrolyte, Proc. Natl. Acad. Sci. U. S. A 114 (5) (2017) 834–839.
[33] H. Jiao, C. Wang, J. Tu, D. Tian, S. Jiao, A rechargeable Al-ion battery: Al/molten AlCl3-urea/graphite, Chem. Commun. 53 (15) (2017) 2331–2334.
[34] Y. Song, S.Q. Jiao, J.G. Tu, J.X. Wang, Y.J. Liu, H.D. Jiao, et al., A long-life rechargeable Al ion battery based on molten salts, J. Mater. Chem. A 5 (3) (2017) 1282–1291.
[35] J.G. Tu, S.B. Wang, S.J. Li, C. Wang, D.B. Sun, S.Q. Jiao, The effects of anions behaviors on electrochemical properties of Al/graphite rechargeable aluminum-ion battery via molten AlCl3-NaCl liquid electrolyte, J. Electrochem. Soc. 164 (13) (2017) A3292–A3302.
[36] C.-Y. Chen, T. Tsuda, S. Kuwabata, C.L. Hussey, Rechargeable aluminum batteries utilizing a chloroaluminate inorganic ionic liquid electrolyte, Chem. Commun. 54 (33) (2018) 4164–4167.
[37] Z.J. Yu, S.Q. Jiao, S. Li, X.D. Chen, W.L. Song, T. Teng, et al., Flexible stable solid-state Al-ion batteries, Adv. Funct. Mater. 29 (1) (2019) 1806799.
[38] X.Z. Dong, C.X. Lu, L.Y. Wang, P.C. Zhou, D.H. Li, L. Wang, et al., Polyacrylonitrile-based turbostratic graphite-like carbon wrapped silicon nanoparticles: a new-type anode material for lithium ion battery, RSC Adv. 6 (16) (2016) 12737–12743.
[39] H.P. Lei, J.G. Tu, Z.J. Yu, S.Q. Jiao, Exfoliation mechanism of graphite cathode in ionic liquids, ACS Appl. Mater. Interfaces 9 (42) (2017) 36702–36707.
[40] J.Z. Wang, K.K. Manga, Q.L. Bao, K.P. Loh, High-yield synthesis of few-layer graphene flakes through electrochemical expansion of graphite in propylene carbonate electrolyte, J. Am. Chem. Soc. 133 (23) (2011) 8888–8891.
[41] Z.L. Zhou, N. Li, Y.Z. Yang, H.S. Chen, S.Q. Jiao, W.L. Song, et al., Ultra-lightweight 3D carbon current collectors: constructing all-carbon electrodes for stable and high energy density dual-ion batteries, Adv. Energy Mater. 8 (26) (2018) 1801439.
[42] C.J. Pan, C.Z. Yuan, G.Z. Zhu, Q. Zhang, C.J. Huang, M.C. Lin, et al., An operando X-ray diffraction study of chloroaluminate anion-graphite intercalation in aluminum batteries, Proc. Natl. Acad. Sci. U. S. A 115 (22) (2018) 5670–5675.
[43] P. Wang, H.S. Chen, N. Li, X.Y. Zhang, S.Q. Jiao, W.L. Song, et al., Dense graphene papers: toward stable and recoverable Al-ion battery cathodes with high volumetric and areal energy and power density, Energy Storage Mater. 13 (1) (2018) 103–111.
[44] P. Simon, Y. Gogotsi, B. Dunn, Where do batteries end and supercapacitors begin? Science 343 (6176) (2014) 1210–1211.